IIE Transactions
Publication details, including instructions for authors and subscription information:
http://www.informaworld.com/smpp/title~content=t713772245

Gaussian process method for form error assessment using coordinate measurements

Haifeng (Heidi) Xia [a]; Yu Ding [a]; Jyhwen Wang [b]
[a] Department of Industrial and Systems Engineering, Texas A&M University, College Station, TX, USA [b] Department of Engineering Technology and Industrial Distribution, Texas A&M University, College Station, TX, USA

Online Publication Date: 01 October 2008

To cite this Article (Heidi) Xia, Haifeng, Ding, Yu and Wang, Jyhwen(2008)'Gaussian process method for form error assessment using coordinate measurements',IIE Transactions,40:10,931 — 946

To link to this Article: DOI: 10.1080/07408170801971502

URL: http://dx.doi.org/10.1080/07408170801971502

IIE Transactions (2008) **40**, 931–946

ISSN: 0740-817X print / 1545-8830 online
DOI: 10.1080/07408170801971502

Gaussian process method for form error assessment using coordinate measurements

HAIFENG (HEIDI) XIA[1], YU DING[1,*] and JYHWEN WANG[2]

[1]*Department of Industrial and Systems Engineering and* [2]*Department of Engineering Technology and Industrial Distribution, Texas A&M University, College Station, TX 77843, USA*
E-mail: yuding@iemail.tamu.edu

Received April 2007 and accepted December 2007

A Gaussian process method for modeling and assessing form errors is presented. The Gaussian process method decomposes a geometric feature into three components: designed geometric form, systematic manufacturing errors and random manufacturing errors. It models the systematic manufacturing errors as a spatial model using a Gaussian correlation function and models the random manufacturing errors as independent identically distributed noises. Based on a handful of coordinate measurements, the Gaussian process model reconstructs the part surface and assesses the form error better than traditional methods. The Gaussian process method also provides an empirical distribution of the form error, allowing engineers to quantify the decision risk on part acceptance. This method works for generic geometric features. The method is implemented on two common features: a straight and a round feature. Simulated datasets as well as actual coordinate measuring machine data are used to demonstrate the improvement achieved by the proposed method over the traditional approaches.

Keywords: Spatial model, Gaussian process, form tolerance, systematic manufacturing error, random manufacturing error

1. Introduction

Manufacturing operations are rarely perfect, so manufactured features inevitably deviate from their nominal design. This deviation is known as manufacturing error. Designers assign tolerances to specify the allowable range of manufacturing errors. If the tolerance is used to control the errors associated with a part dimension, e.g., the radius of a shaft, it is known as the dimensional tolerance; if the tolerance is used to control errors associated with geometric form, e.g., the straight and round geometric features shown in Fig. 1, it is known as the geometric tolerance or form tolerance. Geometric features tend to be more difficult to assess and control, but their integrity is closely related to good quality and correct functioning of a part (please refer to the example of automotive transmission in Woo and Hsieh (1997)).

In order to ensure the geometric integrity of a manufactured part, one needs to first assess the form error using coordinate measurements, and then to compare it with the associated tolerance requirement. For this reason, form error assessment is crucial in controlling form errors and subsequently ensuring the quality and reliability of the part. Our goal here is to study methods that can help assess the form error of geometric features using measurements from a Coordinate Measuring Machine (CMM).

Form error assessment using CMM measurements has been extensively studied. Dowling *et al*. (1997) surveyed the related literature prior to 1997. This survey paper discussed two major ideas: the Minimum Zone (MZ) method and the Orthogonal Least Squares (OLS) method. The MZ method finds the maximum inscribing and minimum circumscribing features that bound all the CMM data and uses the orthogonal width to estimate the form error. The OLS method fits an ideal feature to CMM data by minimizing the sum of squared orthogonal residuals and uses the range of the resulting orthogonal residuals to estimate the form error. Most papers surveyed in Dowling *et al*. (1997) provided algorithms to realize the two ideas for various kinds of geometric features. Dowling *et al.* (1997) also discussed some variants of the OLS method, which use a different objective function, e.g., the least average deviation used in Shunmugam (1987, 1991) and Namboothiri and Shunmugam (1998), which is supposed to be more robust in the presence of measurement outliers.

The post-1997 research output leaned towards searching for efficient/robust algorithms for the MZ method. The proposed methods include the characteristic point-based method (Deng *et al*., 2003) and minimizing the potential energy (Fan and Lee, 1999). Another approach is the exact

*Corresponding author

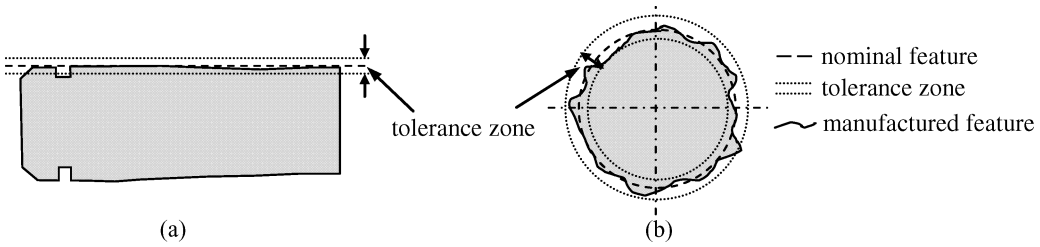

Fig. 1. Illustration of: (a) a straight geometric feature and its form tolerance zone; and (b) a round geometric feature and its tolerance zone.

MZ solution of a geometric feature (e.g., sphericity), as discussed in Huang (1999a) and Chen and Liu (2000). Since it is computationally demanding to find exact MZ solutions using traditional methods such as the convex hull and Voronoi diagram approaches, attention has been focused on how to improve the efficiency of finding the exact MZ (Samuel and Shunmugam, 1999, 2000; Huang, 1999b) and on developing efficient approximation alternatives (Suen and Chang, 1997; Weber *et al*., 2002; Zhu *et al*., 2004). One particularly interesting approach is the zone-fitting method proposed by Choi and Kurfess (1999a, 1999b). The zone-fitting method attempts to verify the form error conformance by transforming all the CMM data back to the design tolerance zone via an optimization routine. It is computationally less demanding than geometry-based methods and is easier to implement for different types of features.

Dowling *et al*. (1997) pointed out several open issues in form error assessment for geometric features. One important issue is how to incorporate the systematic manufacturing errors into a modeling and assessment procedure. Manufacturing errors are always stochastic in nature. In the literature, however, the term *random manufacturing error* generally refers to identically independently distributed (i.i.d.) random deviations from an ideal form, with the term *systematic manufacturing error* referring to non-i.i.d. deviations. Dowling *et al*. (1997) gave a few examples of systematic manufacturing errors. They also pointed out that systematic manufacturing errors are a common cause of form errors in the real world. Therefore, for a model to be realistic it should incorporate systematic errors. This issue has not been well addressed in the existing body of literature. By not accounting for systematic errors, the estimate of the form error can be significantly different to its actual value. This paper attempts to model systematic errors using a Gaussian process model (a spatial statistical model) (Banerjee *et al.*, 2004) in order to better estimate the form error.

Numerous methods have been used to model systematic errors, including basis function methods to approximate the systematic errors, e.g., a polynomial of different orders (e.g., Yeh *et al*. (1994)) and B-spline functions (e.g., Yang and Menq (1993)). Another approach is to use Fourier analysis to distinguish between the generally low-frequency systematic components and the high-frequency random components (e.g., Henke *et al*. (1999), Cho and Tu (2001) and Desta *et al*. (2003)). These models require a large amount of CMM data in order to be able to estimate the relatively large number of parameters involved in the polynomial or B-spline function approaches or to allow a clean separation of the frequencies in the Fourier analysis approach.

Another line of approaches is to use a spatial statistical model (typically, a Gaussian process model) to represent systematic manufacturing errors (Dowling *et al*. 1993; Yang and Jackman, 2000). The non-parametric nature of Gaussian processes offers an improved flexibility in learning general types of systematic errors over the basis-function fitting method and the Fourier analysis method. This feature makes the spatial statistical model attractive, since people generally do not know the function form or the type of systematic manufacturing error in an actual geometric feature in advance. However, little research on the spatial-model-based approach has been performed and the literature on this topic is sparse. In Dowling *et al*. (1993) and Yang and Jackman (2000), the spatial models require one CMM coordinate measurement to be an explicit function of the other two coordinates. Thus, these models cannot be applied to generic geometric features, such as a circle, where one coordinate cannot be expressed as an explicit function of the other two.

Our paper continues this line of research and improves the modeling capability and form error assessment. We first present a Gaussian Process (GP) model that does not require one coordinate to be expressed as an explicit function of other coordinates. We also model both systematic errors (using a spatially correlated term) and random errors (using a spatially uncorrelated term). In contrast, both Dowling *et al*. (1993) and Yang and Jackman (2000) did not include spatially uncorrelated errors. This might not be reasonable if the considered manufacturing process produces both low-frequency systematic errors (because of machine tool wear) and high-frequency random errors (because of machine vibration). In addition, the GP model produces a distribution of the geometric surface, which we subsequently use to estimate an empirical distribution of the form error. The empirical distribution reflects the estimation uncertainty (resulting from the sampling and modeling uncertainty)

and can help quantify the risk of a part not being accepted. Dowling *et al.* (1993) and Yang and Jackman (2000) used one predicted surface to estimate the form error and to decide on accepting or rejecting a part. They did not provide uncertainty information about the form error assessment.

This paper is organized as follows. Section 2 presents the overall structure of the proposed GP model. Section 3 illustrates the procedure to determine the geometric form component in the GP model for a generic feature. Section 4 discusses the GP model formulation and how to estimate the form error. Section 5 compares the proposed GP method with existing methods on two specific geometric features, using both simulated data and real CMM measurements. Section 6 concludes the paper.

2. GP model for form error assessment

When magnified, the surface of a manufactured part looks just like a geographic terrain (please see Stout *et al.* (1990) for the topography of a variety of machined surfaces). This analogy motivates applying a spatial statistical method to represent a manufactured geometric feature. A CMM measurement of an actual geometric feature can be decomposed into three portions (as shown in Fig. 2): a global trend portion, which follows the shape of the feature as defined by its designed form; a spatially *correlated* portion (when the systematic error exists, the measurements in close proximity on a surface show strong correlation); and a spatially *uncorrelated* portion, i.e., the random error portion. As such, we model the CMM measurements as arising from systematic errors and random errors added to an ideal geometric form.

Before writing down the GP model for a part geometry, we need to specify the inputs and the response variable for the model. Recall that the previous GP models require that one coordinate must be expressed in terms of the other coordinates. This is because those GP models used one or two coordinates, e.g., x and/or y, as inputs, and the remaining coordinate, e.g., z, as the response. In order to enable our GP model to be applicable to generic geometric features, we redefine the inputs and the response variables.

Let us consider the measuring mechanism of a computer-controlled CMM. The machine takes the nominal position to be measured, $\mathbf{n}_i$, from an operator (via a computer interface) or a database storing the predetermined position information. Then it calculates the approach direction $\mathbf{v}_i$ for the measuring probe to travel and directs the probe to retrieve the coordinates, denoted by $\mathbf{a}_i$, of a point on the actual geometric feature. This mechanism indicates that the input is $\mathbf{n}_i$ and the response is $\mathbf{a}_i$. Essentially, we map all the points on an ideal geometric form to the actual manufactured feature. Our GP model is set up to capture the mapping between the two surfaces. The advantage is that when we use the nominal position $\mathbf{n}_i$ as the input variable, it works for any type of geometric feature and thus avoids the restriction required by the previous GP models.

The new response $\mathbf{a}_i$ is typically a vector, for example, for a three dimensional feature, $\mathbf{a}_i = [x_i, y_i, z_i]$. A multivariate GP model is obviously more difficult to handle than a univariate model. Thus, we want to further reduce the multivariate response into a single response variable. Here, we adopt the strategy used by Hulting (1997), who suggested projecting the value of $\mathbf{a}_i$ onto the probe approach direction $\mathbf{v}_i$ (usually the norm direction to the local surface) and using the resulting value as the response. As such, our GP model can be written as:

$$z_i \equiv \mathbf{a}_i^{\mathrm{T}} \mathrm{v}_i = \mathbf{f}(\mathbf{n}_i, \boldsymbol{\beta})^{\mathrm{T}} \mathbf{v}_i + \eta(\mathbf{n}_i) + \varepsilon(\mathbf{n}_i), \tag{1}$$

where z_i is the cth CMM observation projected onto the $\mathbf{v}_i$ direction, $\mathbf{f}(\mathbf{n}_i, \boldsymbol{\beta})$ corresponds to the ideal geometric form that engineers design, $\eta(\mathbf{n}_i)$ is the systematic manufacturing error, modeled by a spatially correlated term, and $\varepsilon(\mathbf{n}_i)$ is the random error, modeled by the spatially uncorrelated term. Generally, the random error includes both random manufacturing errors and measurement noises. For the time being, we assume that the measurement errors are negligible and then attribute the second error term $\varepsilon(\mathbf{n}_i)$ entirely to the random manufacturing error. We will discuss what this assumption implies later.

The function form of $\mathbf{f}(\cdot, \cdot)$ can be decided by the shape of a geometric feature, known from the part's design. The value of $\mathbf{f}(\mathbf{n}_i, \boldsymbol{\beta})$ incorporates the actual position of the part, which may undergo a rigid-body motion during the fixturing process, and the changes in dimensions of the part. In other words, β includes two factors: $\boldsymbol{\beta} = (\boldsymbol{\theta}, \boldsymbol{\phi})$, where $\boldsymbol{\theta}$ includes the parameters characterizing the rigid-body motion and $\boldsymbol{\phi}$ includes the dimension parameters (e.g., the radius of a round part). Therefore, the $\mathbf{f}(\mathbf{n}_i, \boldsymbol{\beta})$ can incorporate dimensional errors, for instance, $\boldsymbol{\phi}$ can denote the

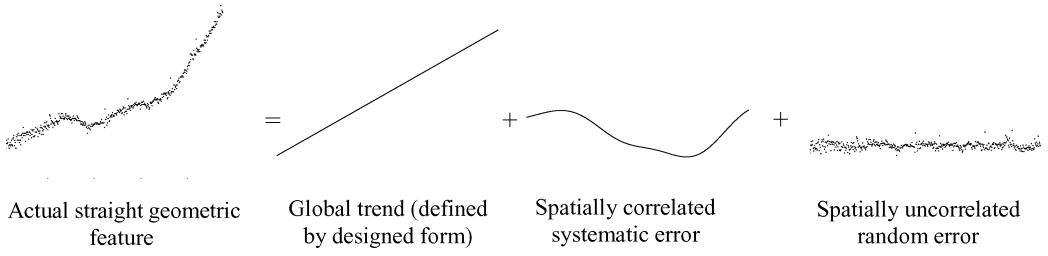

Fig. 2. Decomposition of CMM measurements of a manufactured straight geometric feature.

radius value of an actual part, which may be different from the design value. However, $\mathbf{f}(\mathbf{n}_i, \boldsymbol{\beta})$ still represents the *ideal* geometric form because a deviation in the dimension parameter ϕ does not affect the form error. In other words, a smaller circle could still be a perfect circle.

In model (1), the random error $\varepsilon(\cdot)$ is modeled as i.i.d. $N(0, \sigma_\varepsilon^2)$. The systematic error $\eta(\cdot)$ is assumed to be a GP independent of $\varepsilon(\cdot)$, and of zero-mean and covariance function $\text{cov}(\eta(\mathbf{n}_i), \eta(\mathbf{n}_j)) = \sigma_\eta^2 R(\upsilon, \mathbf{n}_i - \mathbf{n}_j)$, where $R(\upsilon, \cdot)$ is the correlation function with hyper-parameter υ. The rationale behind this is that the systematic departures from the ideal geometric shape can be regarded as a sample path of a (suitably chosen) GP $\eta(\cdot)$. The choice of correlation function $R(\upsilon, \cdot)$ reflects the characteristics of the systematic manufacturing errors. When making the choice for $R(\upsilon, \cdot)$, we also need to consider the scarcity of the data, that is, when a CMM is used to measure a part, the sample size is typically not large. Hence, it would not serve us well if our GP model includes too many parameters to be estimated.

For this reason, we adopt an isotropic Gaussian correlation function, which is widely used in spatial statistics, as follows:

$$R(\upsilon, \mathbf{n}_i - \mathbf{n}_j) = \exp\{-(\upsilon||\mathbf{n}_i - \mathbf{n}_j||_2)^2\}, \qquad (2)$$

where $||\cdot||_2$ denotes Euclidean distance and υ is the scale parameter controlling how quickly the correlation decays as the between-point distance increases. The isotropic Gaussian correlation function has only one unknown parameter υ. Past experience indicates that this correlation function is able to model various spatial features (Zimmerman and Harville, 1991; Gaudard *et al.*, 1999). Our experience also indicates that the Gaussian correlation function appears reasonable for a number of manufactured geometric features. Of course, when the data suggest that for some particular part/feature the spatial correlations are significantly different from Equation (2), this isotropic assumption can be relaxed by including different parameters to control the spatial correlation scale for different directions.

There have been some research reports on modeling more general variance–covariance structures of spatially correlated measurements. For example, Chang and Ho (2001) proposed a correlation model for lattice-structured CMM measurements on a part surface. They assumed that the overall correlation is the product of the row-wise and column-wise correlations and that the CMM measurements in a row or column follow an autoregressive moving average process. This line of research is a valuable contribution to the modeling of systematic manufacturing errors, since a correct variance–covariance structure is essential to a GP model. Under the circumstance that a Gaussian correlation function does not adequately reflect the correlation in the data, the correlation structure proposed in Chang and Ho (2001) could be a good alternative.

The parameters for the GP model are $\boldsymbol{\varphi} \equiv \{\boldsymbol{\beta}, \sigma_\eta^2, \sigma_\varepsilon^2, \upsilon\}$. In practice, engineers use a CMM to measure from one part m data points $\{\mathbf{n}_i, z_i\}_{i=1,\ldots,m}$, and use them to estimate the unknown parameters $\boldsymbol{\varphi}$. Plugging the estimated values for the parameters $\boldsymbol{\varphi}$ into the GP model, engineers can use it to predict the actual coordinate at a not yet measured location and to reconstruct the entire geometric feature. Finally, engineers can assess the form error of the geometric feature using the reconstructed geometric feature. The overall procedure is shown in Fig. 3, where GP($\cdot$, $\cdot$) denotes a Gaussian process with the specified mean and covariance matrix.

3. Determination of the ideal geometric form

In order to fully specify the GP model in Equation (1), this section presents a procedure to determine the ideal geometric form $\mathbf{f}(\mathbf{n}_i, \boldsymbol{\beta})^{\mathrm{T}}\mathbf{v}_i$ for generic geometric features. The procedure follows an idea first proposed by Hulting (1997) when discussing a manufacturing part model; we repeat some of Hulting's original description here in order to make this paper a self-contained piece and to provide a basis for latter discussions.

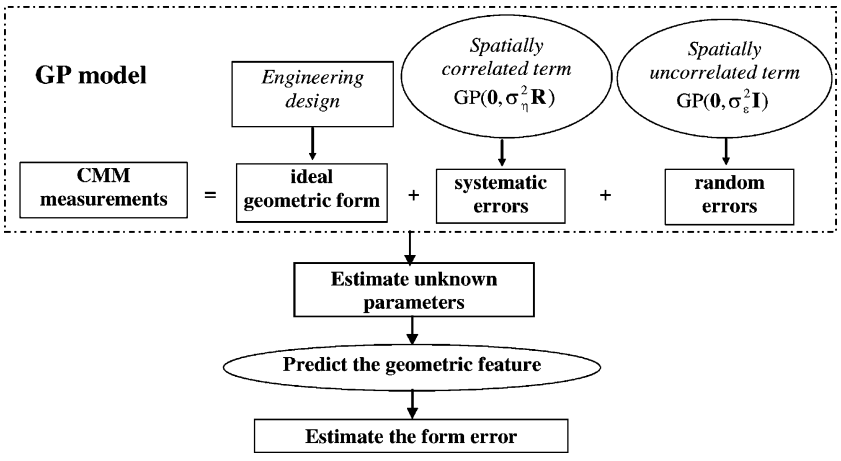

Fig. 3. Procedure of the GP modeling and form error assessment.

Consider a process in which a CMM measures a manufactured part with a general geometric shape, represented by $M(\boldsymbol{\theta}, \boldsymbol{\phi})$, the same notation is used by Hulting, where $\boldsymbol{\theta}$ and $\boldsymbol{\phi}$ follow the same meaning as we explained in Section 2. Denote the nominal design values for the dimension parameters by $\boldsymbol{\phi}^*$. As such, $M(\mathbf{0}, \boldsymbol{\phi}^*)$ represents the designed feature that has the nominated sizes and is perfectly aligned with the CMM reference coordinate. $M(\boldsymbol{\theta}, \boldsymbol{\phi})$ has the same geometry as $M(\mathbf{0}, \boldsymbol{\phi}^*)$ but differs from it in terms of a rigid-body motion and some dimension change. Therefore, $M(\boldsymbol{\theta}, \boldsymbol{\phi})$ represents the ideal form, the same as $\mathbf{f}(\cdot, \cdot)$. More specifically, $\mathbf{f}(\mathbf{n}_i, \boldsymbol{\beta})$ is a point on $M(\boldsymbol{\theta}, \boldsymbol{\phi})$ (recall that $\boldsymbol{\beta} = (\boldsymbol{\theta}, \boldsymbol{\phi})$). As we mentioned before, for a given part, the function form of $M(\cdot,\cdot)$ or that of $\mathbf{f}(\cdot, \cdot)$ is known from the computer-aided design model.

During a coordinate measuring process, $M(\boldsymbol{\theta}, \boldsymbol{\phi})$ only slightly deviates from $M(\mathbf{0}, \boldsymbol{\phi}^*)$ in both location and dimension size. The dimension aspect is easy to understand since a manufacturing process supposedly produces the required dimensions with reasonable accuracy. The location aspect can be understood as follows. A CMM can set up its reference coordinate through *soft fixturing* (Hulting 1995), i.e., it first gets a few reference points on the part to estimate where the part is located and then adapts its reference coordinate to the estimated location.

Determining $\mathbf{f}(\mathbf{n}_i, \boldsymbol{\beta})$ requires solving some geometry equation for a given point $\mathbf{n}_i$. When a CMM is directed to measure a point $\mathbf{n}_i$, it will automatically calculate its path, the approach direction $\mathbf{v}_i$, based on its knowledge of the nominal surface. ($\mathbf{v}_i$ is usually the norm direction to the nominal surface $M(\mathbf{0}, \boldsymbol{\phi}^*)$ since the true shape and location are never known.) As it moves along the path the probe will touch the actual manufactured surface and return the measurement value $\mathbf{a}_i$. Geometrically, $\mathbf{f}(\mathbf{n}_i, \boldsymbol{\beta})$ is an intersection point of the geometric shape $M(\boldsymbol{\theta}, \boldsymbol{\phi})$ and the line passing through $\mathbf{n}_i$ and $\mathbf{n}_i + \mathbf{v}_i$. Therefore, both $\mathbf{a}_i$ and $\mathbf{f}(\mathbf{n}_i, \boldsymbol{\beta})$ lie on the line through $\mathbf{n}_i$ and $\mathbf{n}_i + \mathbf{v}_i$. If projecting those values along $\mathbf{v}_i$, one will end up with the univariate GP model in Equation (1).

The above discussion outlines how to decide $\mathbf{f}(\mathbf{n}_i, \boldsymbol{\beta})^{\mathrm{T}}\mathbf{v}_i$. However, no general analytical formula can be devised for an arbitrary geometry; engineers will have to go through the following procedure (please refer to Fig. 4 for illustrations).

Step 1. Decide the approach direction $\mathbf{v}_i$ according to $M(\mathbf{0}, \boldsymbol{\phi}^*)$ and $\mathbf{n}_i$, and decide the line function passing through $\mathbf{n}_i$ and $\mathbf{n}_i + \mathbf{v}_i$.

Step 2. Solve for the intersection point(s) between the line function and $M(\boldsymbol{\theta}, \boldsymbol{\phi})$.

Step 3. If there is more than one intersection point, select the one that corresponds to the first intersection on $M(\boldsymbol{\theta}, \boldsymbol{\phi})$ when the CMM probe moves.

Step 4. Then, $\mathbf{f}(\mathbf{n}_i, \boldsymbol{\beta})^{\mathrm{T}}\mathbf{v}_i$ is simply the vector inner product of the coordinates of the intersection point $\mathbf{f}(\mathbf{n}_i, \boldsymbol{\beta})$ and $\mathbf{v}_i$.

The detailed procedures of deciding the ideal geometric form for two specific geometric features, straight and round features, are given in the Appendix.

4. Predictive distribution and probabilistic form error assessment procedure

4.1. *Maximum likelihood estimate for parameter estimation*

Recall that the parameters in GP model (1) are $\boldsymbol{\varphi} \equiv \{\boldsymbol{\beta}, \sigma_\eta^2, \sigma_\varepsilon^2, \upsilon\}$ and the training dataset is $\{\mathbf{n}_i, z_i\}_{i=1,\ldots,m}$. We arrange all the z_i values in $\mathbf{z}_{\mathrm{o}}$, i.e., $\mathbf{z}_{\mathrm{o}} = (z_i)_{i=1,\ldots,m}$, where the subscript "o" implies the *observed* CMM measurements. Given the Gaussian process assumption, the distribution of $\mathbf{z}_{\mathrm{o}}$ conditioned on $\boldsymbol{\varphi} = \{\boldsymbol{\beta}, \sigma_\eta^2, \sigma_\varepsilon^2, \upsilon\}$ is

$$(\mathbf{z}_{\mathrm{o}}|\boldsymbol{\varphi}) \sim N(\mathbf{g}_{\mathrm{o}}(\boldsymbol{\beta}), \mathbf{W}_{\mathrm{o}}), \tag{3}$$

where $\mathbf{g}_{\mathrm{o}}(\boldsymbol{\beta})$ is an $m \times 1$ vector, defined such that its ith element is $g_i(\boldsymbol{\beta}) = \mathbf{f}(\mathbf{n}_i, \boldsymbol{\beta})^{\mathrm{T}}\mathbf{v}_i$, and $\mathbf{W}_{\mathrm{o}} = \sigma_\eta^2\mathbf{R}_{\mathrm{o}} + \sigma_\varepsilon^2\mathbf{I}$ and $\mathbf{R}_{\mathrm{o}}$ is an $m \times m$ matrix, defined such that its (i,j)th elements are $R(\upsilon, \mathbf{n}_i - \mathbf{n}_j)$ in Equation (2).

We employ a Maximum Likelihood Estimator (MLE) to estimate the parameters in the GP model. From Equation (3), the log-likelihood function for $\mathbf{z}_o$ can be written as

$$\begin{aligned} l\big(\boldsymbol{\beta}, \sigma_\eta^2, \sigma_\varepsilon^2, \upsilon\big) &= -\big(\log\big(\det\big(\sigma_\eta^2\mathbf{R}_{\mathrm{o}} + \sigma_\varepsilon^2\mathbf{I}\big)\big) \\ &\quad + (\mathbf{z}_{\mathrm{o}} - \mathbf{g}_{\mathrm{o}}(\boldsymbol{\beta}))^{\mathrm{T}}\big(\sigma_\eta^2\mathbf{R}_{\mathrm{o}} + \sigma_\varepsilon^2\mathbf{I}\big)^{-1}(\mathbf{z}_{\mathrm{o}} - \mathbf{g}_{\mathrm{o}}(\boldsymbol{\beta})) \\ &\quad + m\log(2\pi))/2. \end{aligned} \tag{4}$$

An MLE of $\boldsymbol{\varphi} = \{\boldsymbol{\beta}, \sigma_\eta^2, \sigma_\varepsilon^2, \upsilon\}$ is obtained by maximizing $l(\boldsymbol{\beta}, \sigma_\eta^2, \sigma_\varepsilon^2, \upsilon)$, i.e., $\boldsymbol{\varphi}_{\mathrm{MLE}} = \arg\ \max_{\boldsymbol{\phi}} l(\boldsymbol{\beta}, \sigma_\eta^2, \sigma_\varepsilon^2, \upsilon)$.

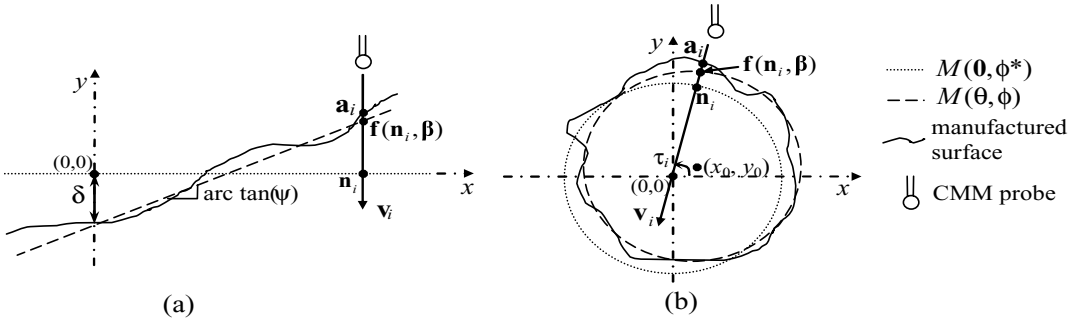

Fig. 4. Demonstrations of deciding the ideal geometric form: (a) for a straight geometric feature; and (b) for a round geometric feature.

We solve it using a gradient-based optimization routine in MATLAB (other similar optimizers can fulfill the task as well). Two more actions are taken to improve the optimization efficiency. One is that we substitute the three parameters $(\sigma_\eta^2, \sigma_\varepsilon^2, \upsilon)$ with $(\exp(\alpha_1), \exp(\alpha_2), \exp(\alpha_3))$. This is because the variance parameters $\sigma_\eta^2, \sigma_\varepsilon^2$ and the correlation hyper-parameter υ can only take positive values and this makes it a constrained optimization. After the transformation, we deal with an unconstrained optimization, which is generally easier to solve. For an unconstrained optimization, we use the MATLAB function fminunc.

For a straight geometric feature, its GP model has a linear mean structure. Thus, we can use a REstricted Maximum Likelihood (REML) estimator, which is supposed to give less biased estimates of covariance parameters (i.e., υ, σ_η^2 and σ_ε^2 in this paper) than MLE. Cressie and Lahiri (1996) proved the asymptotic property of REML estimation for the GP covariance parameters. Wolfinger *et al.* (1994) gave the details for implementing a RMLE for a linear GP model. For a roundness feature, model (1) has a non-linear mean structure so REML estimation is not available. Therefore, we use a MLE for round features.

4.2. *Predictive distribution of geometric surface and form error assessment*

For the purpose of form error assessment, we are ultimately interested in predicting the behavior of the geometric feature based on the observed CMM measurements. We approximate the continuous surface of a geometric feature by a dense set of points on it. Denote by $\{\mathbf{p}_i\}_{i=1:N}$ the dense set of nominal points on a geometric feature, which are deemed representative of the feature. The prediction of the geometry at $\mathbf{p}_i$ is $z(\mathbf{p}_i)$, and we arrange all N predictions in vector $\mathbf{z}_\mathrm{p}$, i.e., $\mathbf{z}_\mathrm{p} = (z(\mathbf{p}_i))_{i=1:N}$, where the subscript "p" implies a prediction. Given the Gaussian process assumption, $\mathbf{z}_\mathrm{p}$ and $\mathbf{z}_\mathrm{o}$ follow a joint multivariate normal distribution:

$$(\mathbf{z}_\mathrm{p}, \mathbf{z}_\mathrm{o}|\boldsymbol{\varphi}) \sim N\left(\begin{pmatrix}\mathbf{g}_\mathrm{p}(\boldsymbol{\beta})\\ \mathbf{g}_\mathrm{o}(\boldsymbol{\beta})\end{pmatrix}, \quad \begin{pmatrix}\mathbf{W}_\mathrm{p} & \mathbf{W}_\mathrm{po}^\mathrm{T}\\ \mathbf{W}_\mathrm{po} & \mathbf{W}_\mathrm{o}\end{pmatrix}\right), \quad (5)$$

where $\mathbf{g}_\mathrm{o}(\boldsymbol{\beta})$ and $\mathbf{W}_\mathrm{o}$ are defined in Equation (3), $\mathbf{g}_\mathrm{p}(\boldsymbol{\beta})$ is an $N \times 1$ vector, defined such that its ith element is $g_i(\boldsymbol{\beta}) = \mathbf{f}(\mathbf{p}_\mathrm{i}, \boldsymbol{\beta})^\mathrm{T}\mathbf{v}_\mathrm{i}$, $\mathbf{W}_\mathrm{po}$ is the covariance matrix between $\mathbf{z}_\mathrm{o}$ and $\mathbf{z}_\mathrm{p}$, and $\mathbf{W}_\mathrm{po} = \sigma_\eta^2\mathbf{R}_\mathrm{po}$; $\mathbf{W}_\mathrm{p}$ is the covariance matrix of $\mathbf{z}_\mathrm{p}$ and $\mathbf{W}_\mathrm{p} = \boldsymbol{\sigma}_\eta^2\mathbf{R}_\mathrm{p} + \boldsymbol{\sigma}_\varepsilon^2\mathbf{I}$. The correlation matrix $\mathbf{R}_\mathrm{po}$ is an $N \times m$ matrix, and its (i,j)th elements are $R(\upsilon, \mathbf{p}_i - \mathbf{n}_j)$; $\mathbf{R}_\mathrm{p}$ is an $N \times N$ correlation matrix, and its (i,j)th elements are $R(\upsilon, \mathbf{p}_i - \mathbf{p}_j)$.

According to the conditional distribution theorem for a multivariate normal distribution (Hardle and Simar, 2003, p .157), we can have that:

$$(\mathbf{z}_\mathrm{p}|\mathbf{z}_\mathrm{o}, \boldsymbol{\varphi}) \sim N(\mathbf{g}_\mathrm{p}(\boldsymbol{\beta}) + \mathbf{W}_\mathrm{po}\mathbf{W}_\mathrm{o}^{-1}(\mathbf{z}_\mathrm{o} - \mathbf{g}_\mathrm{o}(\boldsymbol{\beta})), \mathbf{W}_\mathrm{p} - \mathbf{W}_\mathrm{po}\mathbf{W}_\mathrm{o}^{-1}\mathbf{W}_\mathrm{po}^\mathrm{T}). \quad (6)$$

Equation (6) provides the predictive distribution of the discretized geometric feature based on the observed CMM measurements $\mathbf{z}_\mathrm{o}$. The negative amount $\mathbf{W}_\mathrm{po}\mathbf{W}_\mathrm{o}^{-1}\mathbf{W}_\mathrm{po}^\mathrm{T}$ in the variance term comes from the observed measurements $\mathbf{z}_\mathrm{o}$ and their correlations with the predicted locations. Basically, the information in the CMM observations helps reduce the uncertainty when predicting the geometric feature. The more CMM data or the stronger the correlation between $\{\mathbf{p}_i\}_{i=1:N}$ and $\{\mathbf{n}_i\}_{i=1:m}$ is, the less uncertainty remains in the predictive distribution of the geometric feature. In practice, the parameter $\boldsymbol{\varphi} = \{\boldsymbol{\beta}, \sigma_\eta^2, \sigma_\varepsilon^2, \upsilon\}$ is unknown and will be estimated from CMM observations. A common treatment is to plug in the MLE $\hat{\varphi}$ into distribution (6). The predictive distribution with the plugged-in parameter estimates looks like:

$$(\hat{\mathbf{z}}_\mathrm{p}|\mathbf{z}_\mathrm{o}, \hat{\boldsymbol{\varphi}}) \sim N(\mathbf{g}_\mathrm{p}(\hat{\boldsymbol{\beta}}) + \hat{\mathbf{W}}_\mathrm{po}\hat{\mathbf{W}}_\mathrm{o}^{-1}(\mathbf{z}_\mathrm{o} - \mathbf{g}_\mathrm{o}(\hat{\boldsymbol{\beta}})), \hat{\mathbf{W}}_\mathrm{p} - \hat{\mathbf{W}}_\mathrm{po}\hat{\mathbf{W}}_\mathrm{o}^{-1}\hat{\mathbf{W}}_\mathrm{po}^\mathrm{T}), \quad (7)$$

where $\hat{\mathbf{W}}_\mathrm{o} = \hat{\sigma}_\eta^2\hat{\mathbf{R}}_\mathrm{o} + \hat{\sigma}_\varepsilon^2\mathbf{I}$, $\hat{\mathbf{W}}_\mathrm{p} = \hat{\sigma}_\eta^2\hat{\mathbf{R}}_\mathrm{p} + \hat{\sigma}_\varepsilon^2\mathbf{I}$, $\hat{\mathbf{W}}_\mathrm{po} = \hat{\sigma}_\eta^2\hat{\mathbf{R}}_\mathrm{po} + \hat{\sigma}_\varepsilon^2\mathbf{I}$ and $\hat{\mathbf{R}}_\mathrm{o}, \hat{\mathbf{R}}_\mathrm{p}, \hat{\mathbf{R}}_\mathrm{po}$ are the correlation matrix with hyper-parameter value of $\hat{\upsilon}$ plugged in.

We can reconstruct the geometric feature by drawing a sample from the multivariate distribution specified in Equation (7), which is a realization of the discretized geometric feature. The density of prediction locations is supposedly much higher than the actual CMM measurements, i.e., $N \gg m$, and the CMM measuring sites $\{\mathbf{n}_i\}_{i=1:m}$ are usually a subset of the prediction sites $\{\mathbf{p}_i\}_{i=1:N}$. That allows the reconstructed surface to provide a closer representation of the geometric feature than the handful of CMM observations scattered over the surface. Once a surface is predicted (or reconstructed), the form error of the feature, denoted by h, is estimated through finding the maximum inscribing and minimum circumscribing geometry that bounds all points on the predicted surface (known as the Taylor's principle (Dowling *et al.*, 1997)).

To account for the uncertainty in both the data and model, we need to repeat the above procedure T times. T needs to be a big number to ensure a good approximation, and we use $T = 10\,000$ for the study in Section 5. Figure 5(a) shows a 95% predictive band of the predicted surface and the average predicted surface, together with the measured and true values of the surface (this is a simulated case so we know the true surface).

Finally, we have T estimates of the form error, $\hat{h}_1, \hat{h}_2, \ldots, \hat{h}_T$, each of which is calculated by applying Taylor's principle to an individual predicted surface. Using the T estimates of the form error, we can produce an empirical distribution of h, shown as the histogram in Fig. 5(b). This histogram is an empirical predictive distribution of the form error, given the CMM measurements $\mathbf{z}_\mathrm{o}$ and the GP model. When a large sample is used, the distribution of h is centered around the actual form error. Thus, it makes sense to use the median (denoted as $\hat{h}_{(0.5)}$) of the empirical distribution of h as the final estimate of the form error.

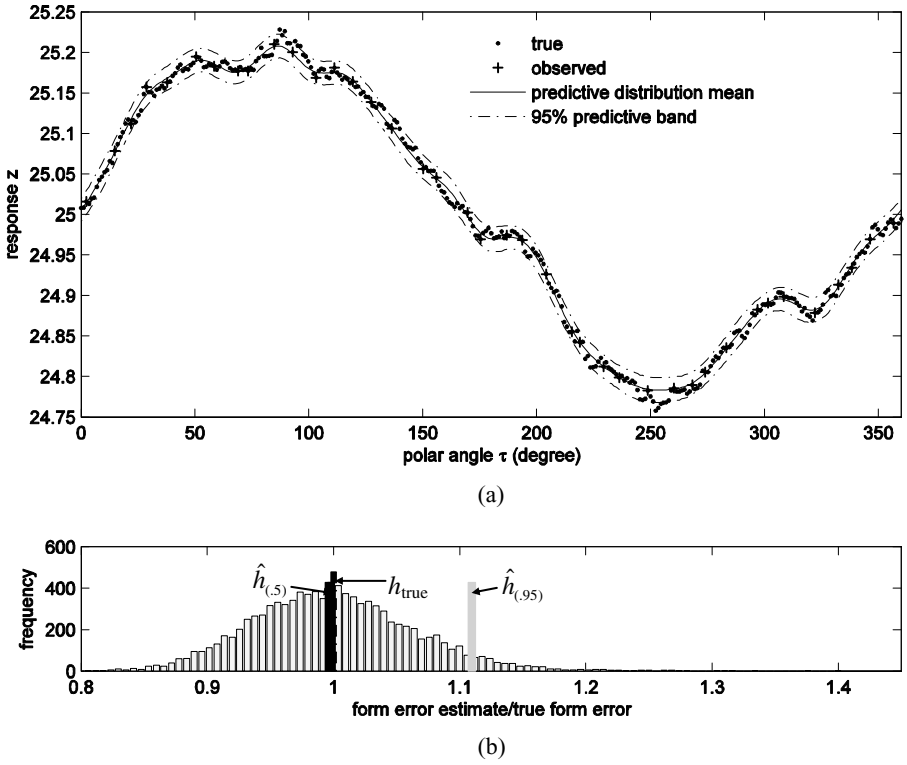

Fig. 5. (a) Predictive distribution for a round geometric feature and (b) the associated form error estimate histogram.

In fact, the predictive distribution of h contains richer information than a point estimate of the form error. It allows engineers to quantify the decision risk on part acceptance. In practice when the sample size is limited, one may want to be more conservative in accepting the part. For example, instead of using the median $\hat{h}_{(0.5)}$, one could use the 95th percentile of the empirical distribution, $\hat{h}_{(0.95)}$, to be compared with a predetermined form tolerance. If $\hat{h}_{(0.95)}$ is smaller than the predetermined form tolerance, one is more than 95% confident that the part form error is less than the form tolerance. Which exact percentile to use can be adjusted based on the functionality requirements and the cost of making a wrong decision.

5. Comparison with traditional methods

This section compares the GP method for form error estimate with the two traditional methods: the MZ method and the OLS method. We choose these two methods as the reference for comparison primarily because they are still the most popular ones in the literature and are widely used in form error assessment software provided by CMM manufacturers.

In this section, we focus on comparing the unbiasness of the form error estimates from the three different methods. We calculate the ratios of the estimated form errors over the true form errors. The true form errors are known for the simulation studies. If the calculated ratio is closer to one, the estimate is less biased. We do not compare the probabilistic decision-making procedure allowed by the predictive distribution of h, because the MZ and OLS methods do not take the uncertainty information into account in their decision-making procedure. However, we believe that it is an advantage of the GP method that it provides distribution information that can quantify the decision risk for industrial practices.

We do not compare the speed of these three methods, because the GP method uses a large number of replications to get the predictive distribution of the form error, while the other two do not. The OLS method only calculates a point estimate and is faster. Finding the exact MZ solution could be computationally demanding, but many fast approximation algorithms are available. In our study here, we actually use the *minimax* estimate to approximate the MZ. The actual computation time of the GP method ranges from tens of seconds to several minutes, which should be acceptable to practitioners.

Section 5.1 performs the comparison using a set of simulated data. We simulate a total of six different manufacturing scenarios for two geometric features: a straight feature and a round feature, with three scenarios for each. For each scenario, different sizes of samples, ranging from eight to 80 for the straight and round features, are used to estimate the form error. The sample size, denoted by m, refers to the number of the measurements taken from different locations on a part.

In Section 5.2, we use a CMM to obtain actual coordinate measurements from two parts with a straight feature and a round feature, respectively. We apply the GP method, the MZ method and the OLS method to estimate form error and other parameters for each of the above cases.

5.1. *Comparison using simulated data*

We follow the following procedures to implement the simulation study for each manufacturing scenario in Section 5.1. (A similar procedure was used by Dowling *et al.* (1995) to compare the performance of the MZ method and the OLS method.)

Step 1. Simulate one single geometric feature.

Step 2. Generate a dense enough set of measurements, a total of N points on the selected geometric feature so that the measurements closely represent the actual geometry. In the simulation, we take a measurement every 0.5 mm. Our experience indicates that this density is considered dense enough by practitioners. Thus, $N = L/0.5$, where L is the length of a straight feature or the circumference of a round feature. Determine the form error h^* from the N points using the MZ method and treat it as the "true" form error.

Step 3. Select m data points from the set of dense measurements and treat them as the CMM measurements of the geometric feature. The m locations and their corresponding observations are chosen using a *maximin* distance Latin hypercube sampling approach; this method makes sure that the m samples evenly spread over the feature space. For more details on the *maximin* distance Latin hypercube sampling procedure, please refer to Santner *et al.* (2003, p. 150).

Step 4. For $m = 8$, 10, 15, 20, 30, 40 and 80, determine the form error estimate and denote by $\hat{h}_{\mathrm{OLS}}(m)$ when using the OLS method, by $\hat{h}_{\mathrm{MZ}}(m)$ when using the MZ method, and by $\hat{h}_{\mathrm{GP}}(m)$ when using the GP method (which is the $\hat{h}_{(0.5)}$ as defined in Section 4).

Step 5. Calculate the estimate ratios, $\hat{h}_{\mathrm{OLS}}(m)/h^*$, $\hat{h}_{\mathrm{MZ}}(m)/h^*$ and $\hat{h}_{\mathrm{GP}}(m)/h^*$. A ratio closer to one indicates a less biased estimate.

Step 6. Repeat Steps (3) to (5) 50 times for each m and generate a box-whisker plot of the form error estimate.

5.1.1. *Straight feature*

In this subsection, we simulate the straight feature. Manufacturing errors of a straight feature usually include surface deflection, waviness and random error. Depending on what manufacturing process is used to produce the feature, one of the errors could dominate in the measurements. For instance, when using a lathe (a turning process) to machine the feature, surface deflection could be more prominent than other types of errors because of the force exerted perpendicularly to the surface. Dowling *et al.* (1995) suggested a generating function for simulating different scenarios of the form of

$$y = \delta + \psi x - \frac{64}{L^6} R(x^3(L-x)^2) + A \sin\left(\frac{2\pi}{\lambda} x\right) + \varepsilon, \quad (8)$$

where the first two terms $\delta + \psi x$ represent the rigid-body motion during a fixturing process, the third term represents the surface deflection, the fourth term is a wave pattern, and the last term is the i.i.d. random error, assumed to be $N(0, \sigma_\varepsilon^2)$. Including an i.i.d. pure random error sometimes creates outliers that jump out of the geometric surface. The existence of such outliers creates an abrupt discontinuity in the geometry and may not accurately reflect the actual surface. To alleviate the discontinuity problem, we use a three-point moving average window to smooth the i.i.d. random error. The meanings of the other parameters in Equation (8) are as follows: L is the length of the straight feature; A is the sinewave amplitude; λ is the wavelength; R is the deflection range. We simulate a feature of length $L =$ 200 mm. Table 1 shows the three simulated manufacturing scenarios, corresponding to a milling, turning and grinding process, respectively. The parameters in Table 1 are determined from the typical process capability associated with each of the manufacturing processes.

5.1.2. *Round feature*

This paper adopts the round feature generator from Desta *et al.* (2003):

$$\begin{aligned} x &= x_0 + (r + A_1 \sin(4\tau) + A_2 \cos(3\tau) + A_3 \sin(7\tau) \\ &\quad + A_4 \cos(10\tau) + \varepsilon) \cos\tau, \\ y &= y_0 + (r + A_1 \sin(4\tau) + A_2 \cos(3\tau) + A_3 \sin(7\tau) \\ &\quad + A_4 \cos(10\tau) + \varepsilon) \sin\tau, \end{aligned} \quad (9)$$

where x_0 and y_0 are the origin of the round feature, r is the radius, τ is the polar angle, $A_1 \sin(4\tau) - A_2 \cos(3\tau) + A_3 \sin(7\tau) + A_4 \cos(10\tau)$ represents the systematic error and the other notations are the same as defined before. Table 2 summarizes three different manufacturing scenarios.

Table 1. Manufacturing scenarios for a straight geometric feature.

	Process characteristics	ϕ*(mm)*	ψ	A*(mm)*	λ*(mm)*	R*(mm)*	σ_ε*(mm)*
Case I	Sinewave dominates (face milling)	0.04	0.02	0.03	20	0.015	0.017
Case II	Deflection dominates (turning)	0.05	0.01	0.005	10	0.025	0.009
Case III	Random errors dominate (grinding)	0.03	−0.01	0	N/A	0	0.003

Table 2. Manufacturing scenarios for a round geometric feature (unit: mm).

	Process characteristics	x_0	y_0	A_1	A_2	A_3	A_4	r	σ_ε
Case I	Three-lobed systematic errors dominate and radius change (turning)	0.2	0.02	N/A	0.03	N/A	N/A	25.03	0.01
Case II	General systematic errors dominate (turning)	0.03	0.2	0.002	−0.015	−0.01	−0.008	25	0.012
Case III	Random errors dominate (turning)	0.01	0.15	N/A	N/A	N/A	0	25	0.017

5.1.3. *Results and discussions*

Figures 6 to 8 show the results of form error estimation for the straight feature, and Figs. 9 to 11 shows the estimation results for the round feature. In each box-whisker plot, the locations of the upper limit, the 75% quantile, the median, the 25% quantile and the lower limit are shown. The crosses outside of the upper and lower limits are usually considered as "outliers".

The dashed line indicates that the estimate of the form error is the same as the true form error (i.e., the estimated ratio is equal to one). In other words, the best method is the one that consistently produces box-whisker plots closest to the dashed line.

From Figs. 6 to 11, we observe the following.

1. The proposed GP method performs significantly better than the OLS and MZ methods when systematic manufacturing errors exist. When the sample size grows larger, the GP method tends to be unbiased. This appears to confirm what we observed in the empirical distribution of form error estimate in Fig. 5(b). By comparison, the MZ and OLS methods tend to underestimate the form error, even when using a relatively large sample size (for example, $m = 40$ or 80). Dowling *et al.* (1995) also mentioned the underestimation of the MZ and OLS methods for straight features. We believe that our form error estimation/assessment benefits from the GP method's

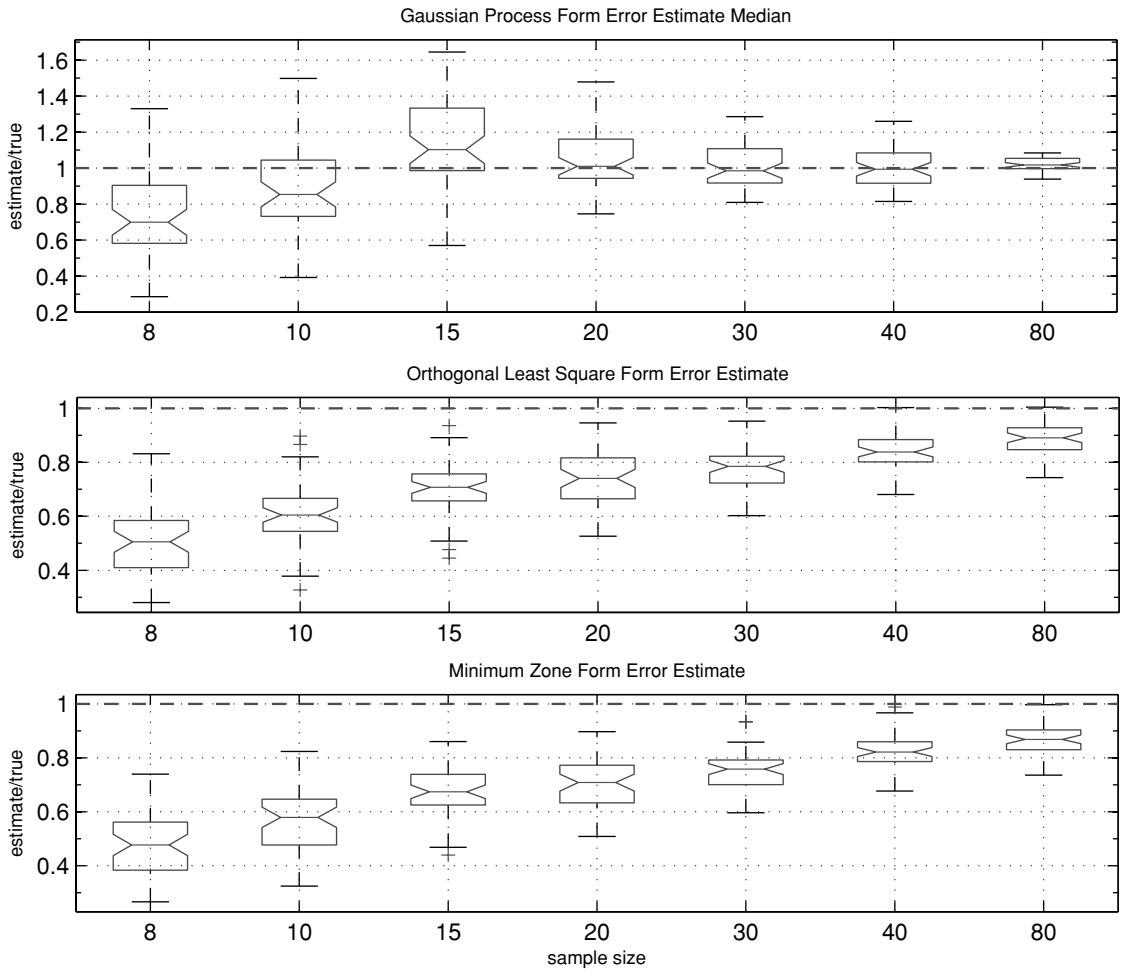

Fig. 6. Form error estimate comparison for a straight feature; case I.

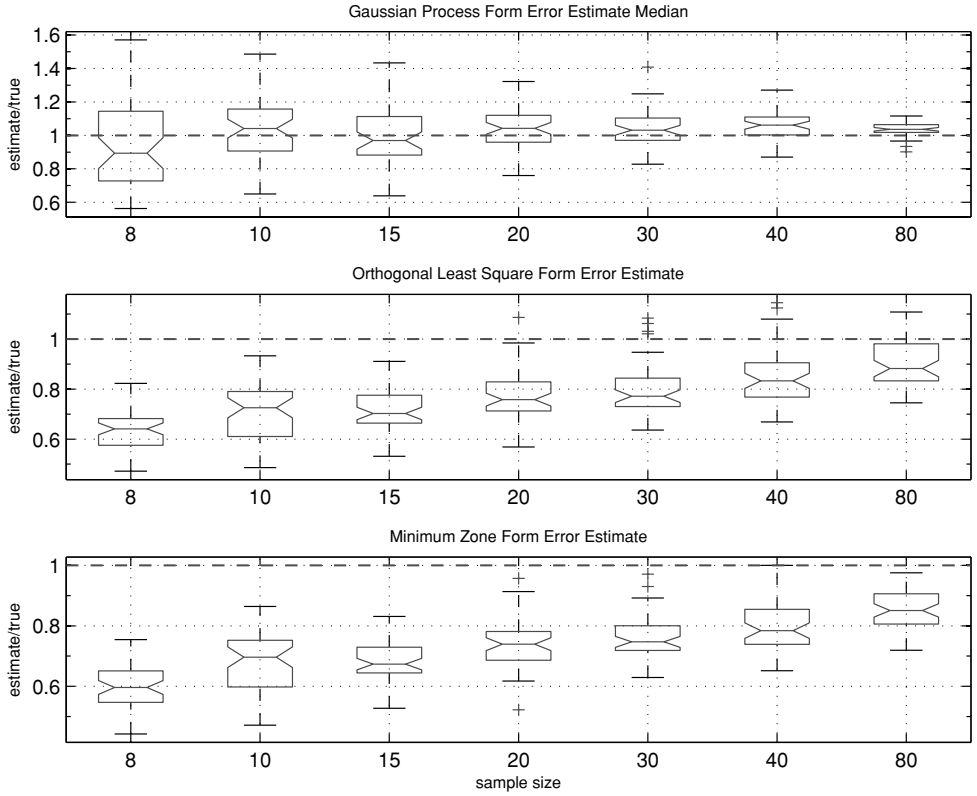

Fig. 7. Form error estimate comparison for a straight feature: case II.

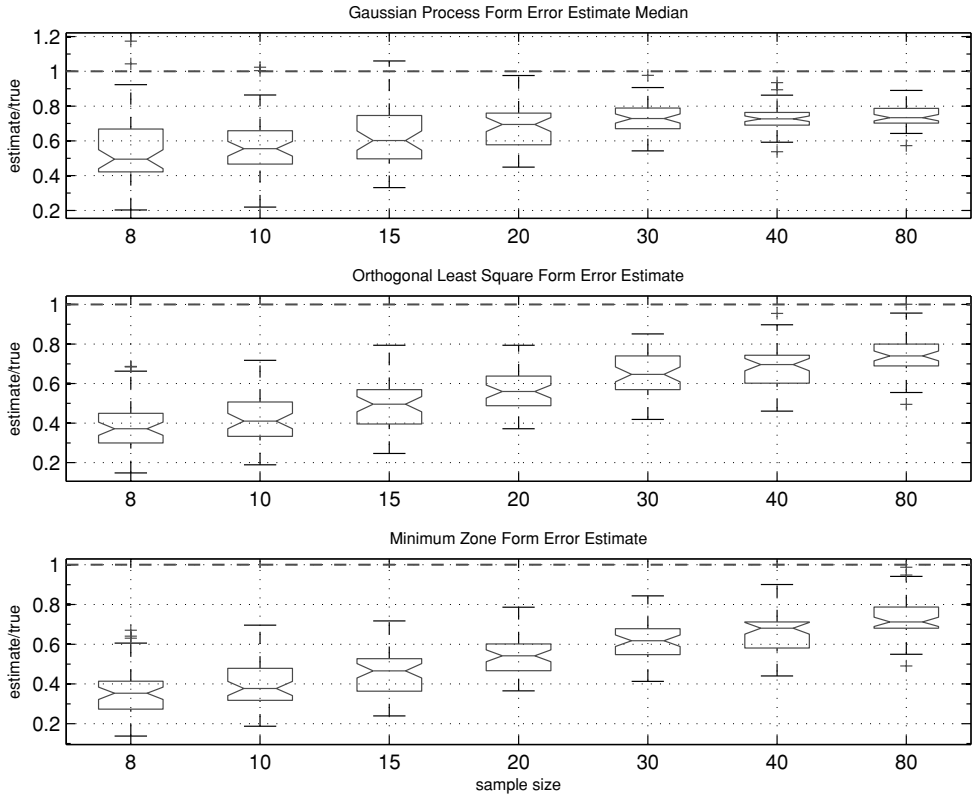

Fig. 8. Form error estimate comparison for a straight feature: case III.

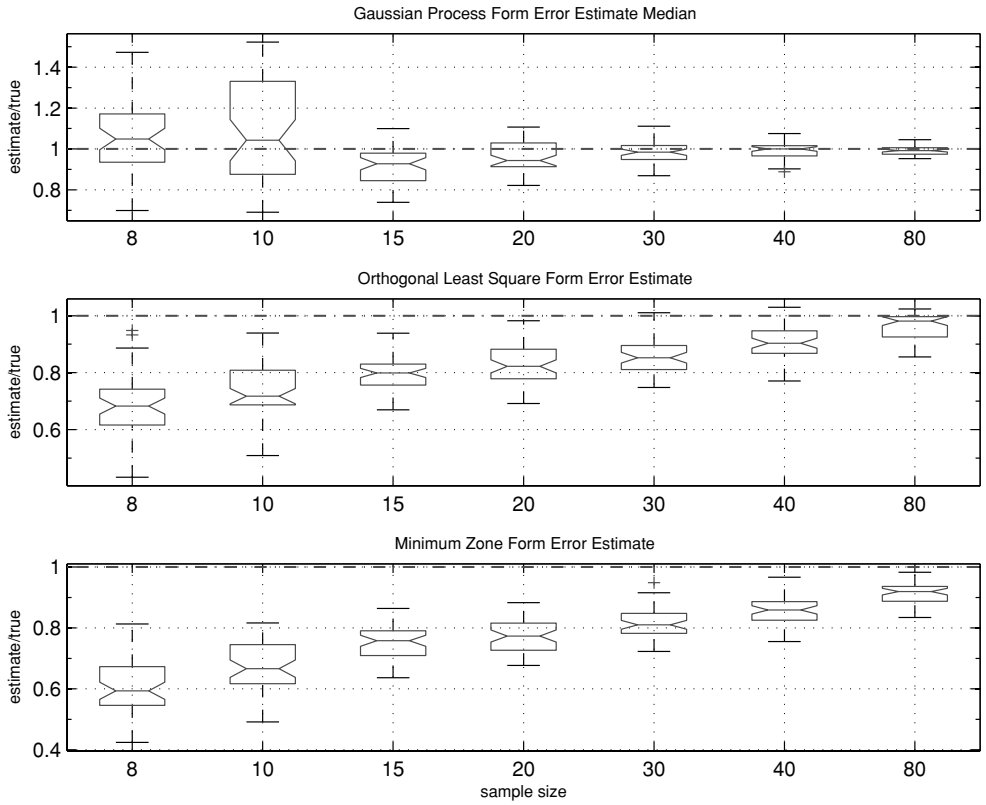

Fig. 9. Form error estimation comparison for a round feature: case I.

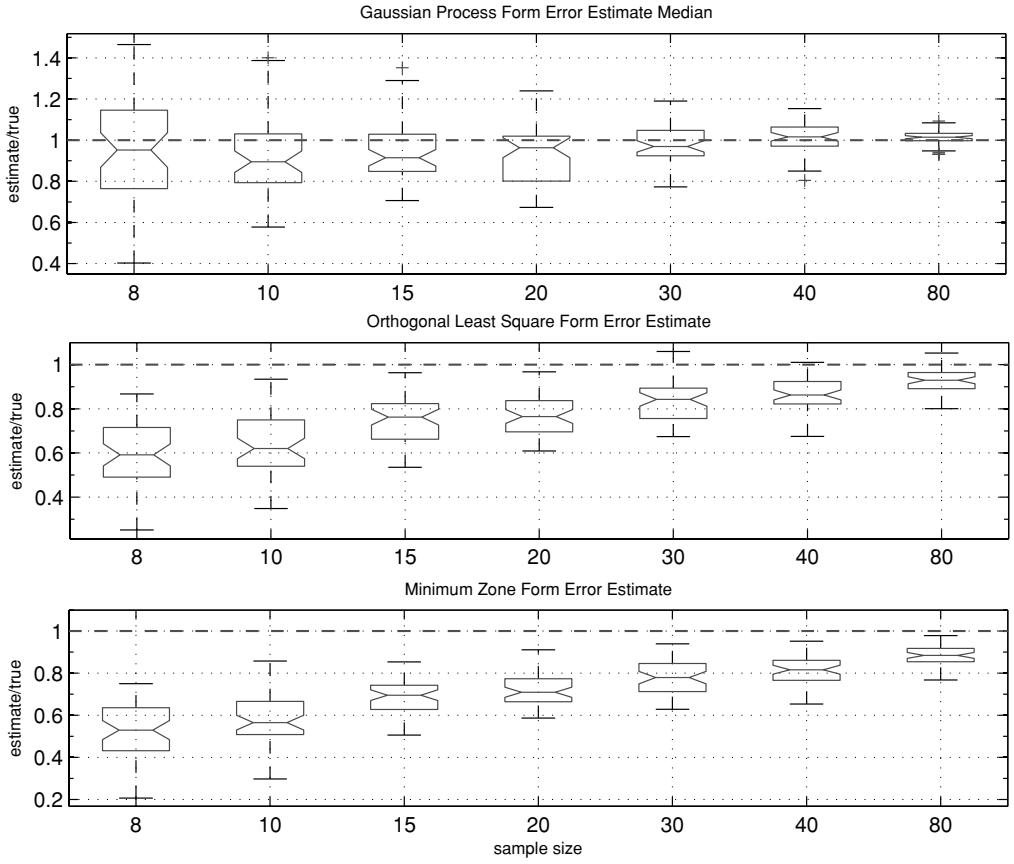

Fig. 10. Form error estimation comparison for a round feature: case II.

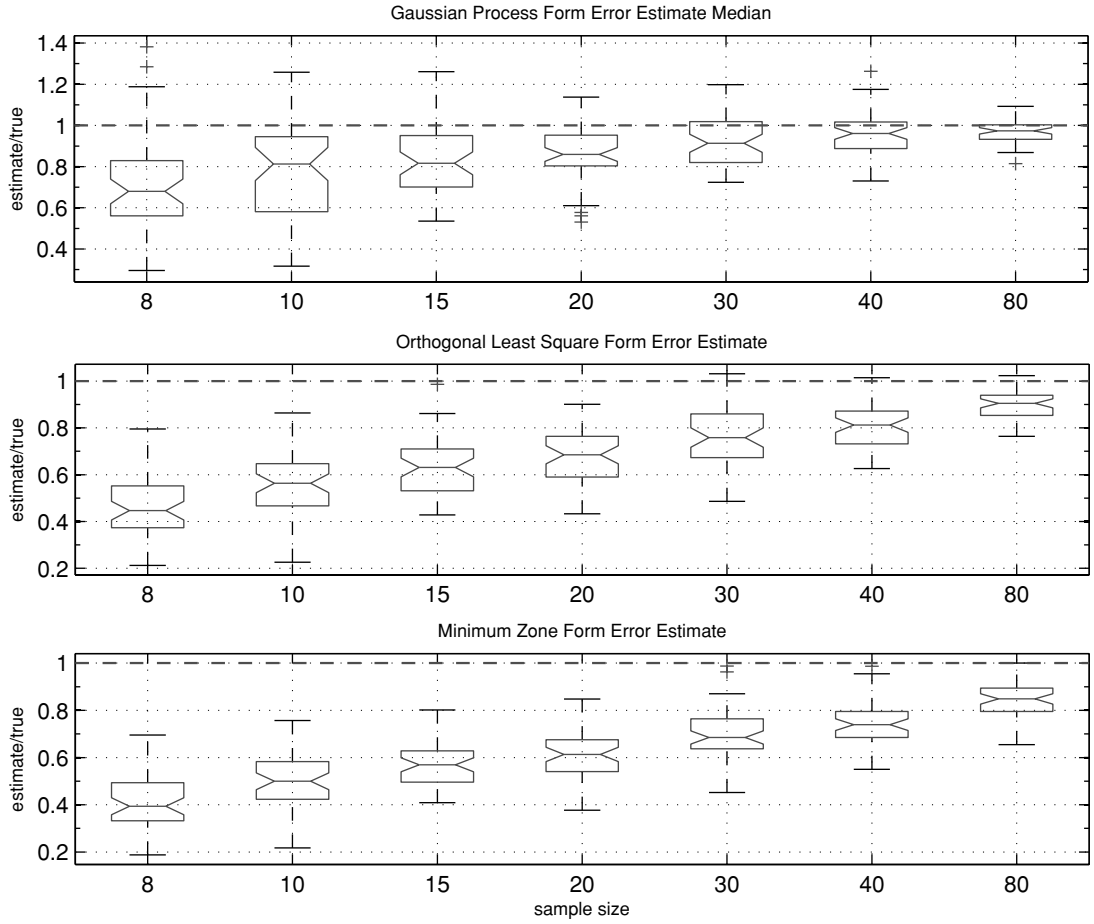

Fig. 11. Form error estimation comparison for a round feature: case III.

ability to capture the systematic manufacturing errors (please refer to Fig. 5(a), where the predicted surface for a round feature is shown), while the other two methods treat the handful of CMM measurements as a complete representation of the entire feature.

2. In the cases when only random manufacturing errors exist (i.e., Figs. 8 and 11), the GP method performs similarly to the OLS method and slightly better than the MZ method. This is expected since the OLS method assumes that the error term consists of i.i.d. random noises. When the systematic error term vanishes, a GP model is essentially the same as an OLS model.
3. The GP method suffers from not having sufficient information when the CMM sample is small as the other two methods do, but to a less degree. Insufficient information from a small sample generally leads to wider predictive distributions, meaning more uncertainty.
4. In our simulations, we decide the smallest sample size according to the number of unknown parameters used in the GP model (which is five for the straight and six for the round features). We start with a sample size roughly 1.5 times that of the number of unknown parameters. The literature is uncertain as to how many samples are required to produce a good prediction. Bernardo *et al.* (1992) suggested using *three observations per parameter* as a rule of thumb for good model performance. That translates to a sample size of 15 and 18, respectively, for the two features. From the simulation results, we

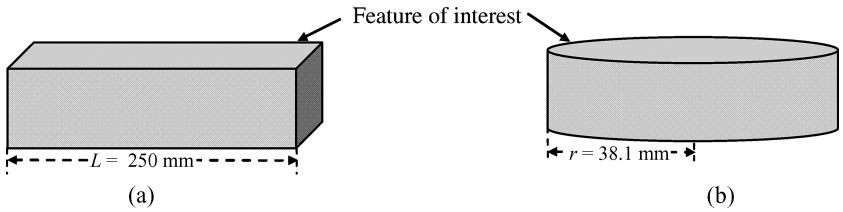

Fig. 12. Sketches of two real parts; (a) a straight feature; and (b) a round feature.

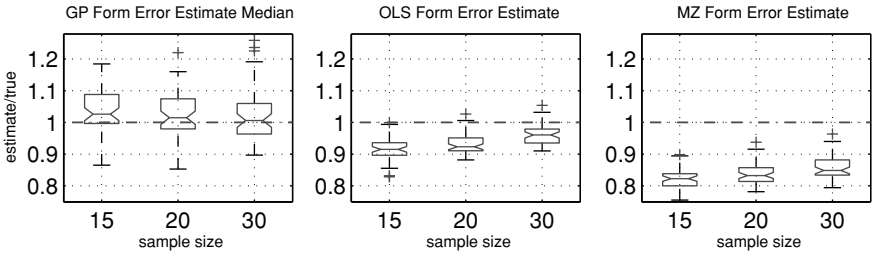

Fig. 13. Form error estimate comparison using real CMM measurements for the straight feature.

observed that the GP method produces reasonably good estimate of form error when the sample size is larger than 15 for straight or larger than 20 for round features. One may argue that a sample of size 15 may be much more than what is typically used in practice; Dowling *et al.* (1997) mentioned that people use three to five points for a line feature and four to eight points for a circle. However, citing the work by Weckenmann *et al.* (1991), Dowling *et al.* (1997) also pointed out that the small sample size practice is not sufficient, and mentioned that a sample of ten to 20 is instead needed for sufficient precision in estimating the errors and parameters. What our simulation suggests appears consistent with the recommendation in Weckenmann *et al.* (1991).

5. In the cases where the number of measurements is fewer than 1.5 times that of the number of unknown parameters, we feel that the GP method may not produce accurate enough predictions so the alternative method should be used.

5.2. *Form error estimate using actual CMM measurements*

We used a CMM to obtain coordinate measurements from two parts. A 250 mm long straight block (Fig. 12 (a)) was manufactured by a face milling process and a cylinder with a 38.1 mm radius (Fig. 12 (b)) was manufactured by a rough turning process. We took dense CMM measurements (i.e., one measurement every 0.5 mm) for both the straight and the round features. In total we took 500 points from the straight feature, and 480 points from the circle. We applied Taylor's principle to the dense CMM measurements, and treated the calculated form error as the true form error h^*. The form error for the straight feature was $h^* = 0.052$ mm, and for the round feature $h^* = 0.43$ mm.

Then, we took a smaller, more practical number, m, of CMM observations for each part to estimate the form error. Again the three methods, GP, OLS and MZ were used. The sample sizes we used are 15, 20 and 30. Figures 13 and 14 summarize the comparison results for the straight feature and round feature, respectively. Consistent with the previous simulation results, the GP-method-based form error estimates the median much better than the other two estimates and appears to be less biased than the OLS and MZ methods.

In addition, we estimated the dimension parameter (only for the round part), and the variance of the random errors. Table 3 shows the estimation results and gives the mean values and the associated standard deviations (in parentheses).

For round features, manufacturing engineers are interested in estimating radius $\hat{r}$ and using it in dimensional quality control. For all the sample sizes, estimates from the GP method and from the OLS method are very close in terms of both the average estimates and the standard deviations. The MZ estimate of $\hat{r}$ deviates more noticeably from the OLS and GP estimates and the standard deviation of the MZ estimate is about three times larger than those of the OLS and GP estimates. This suggests that using the MZ method for parameter estimation might not be a good practice.

The estimated standard deviation of the random error $\hat{\sigma}_\varepsilon$ can be obtained by the GP and OLS methods but not by the MZ method. In fact, every decision in a MZ procedure is deterministic. One may notice that the GP method yields a smaller estimate of $\hat{\sigma}_\varepsilon$ than the OLS method. This is because the OLS method treats all the errors (η and ε) as the random

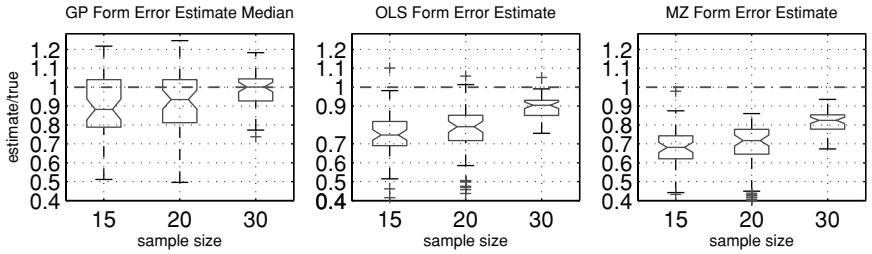

Fig. 14. Form error estimate comparison using real CMM measurements for the round feature.

Table 3. Parameter estimate comparison.

	Straight feature		*Round feature*				
Sample size	$\hat{\sigma}_\varepsilon^{OLS}(\mu m)$	$\hat{\sigma}_\varepsilon^{GP}(\mu m)$	$\hat{\sigma}_\varepsilon^{OLS}(\mu m)$	$\hat{\sigma}_\varepsilon^{GP}(\mu m)$	$\hat{r}_{OLS}(mm)$	$\hat{r}_{MZ}(mm)$	$\hat{r}_{GP}(mm)$
15	15 (0.65)	3.4 (1.1)	93 (18)	21 (12)	38.10 (1.1×10^{-2})	38.07 (3.3×10^{-2})	38.09 (1.2×10^{-2})
20	14 (0.61)	3.4 (1.2)	87 (16)	22 (11)	38.10 (1.3×10^{-2})	38.06 (3.4×10^{-2})	38.10 (1.3×10^{-2})
30	14 (0.48)	3.3 (1.2)	89 (7.4)	18 (9.8)	38.10 (7.1×10^{-3})	38.04 (2.6×10^{-2})	38.10 (6.1×10^{-3})

error and thus may inflate the estimate of $\hat{\sigma}_\varepsilon$. The inflation in estimating $\hat{\sigma}_\varepsilon$ will cause a loss of power in subsequent inferences (Kurfess *et al*., 1996).

Other parameters such as $\hat{\delta}$, $\hat{\psi}$, $\hat{x}_0$ and $\hat{y}_0$ can be estimated as well. These parameters are related to the rigid-body motion of the part during a fixturing process. They are not directly involved in the form error assessment but only work as a compensation of imperfect alignment. These values are indeed small because of the soft-fixturing procedure used in a CMM measuring process. To save space, we do not list them here.

6. Concluding remarks

This paper presents a GP method for form error assessment. Our comparisons show the GP method generally gives a less biased estimate of the form error than the traditional MZ and OLS methods. The simulation results indicate that a sample of 15 or more CMM observations should be used with our GP method, at least for the two geometric features under consideration. This result is consistent with recommendations from previous studies (e.g., Weckenmann *et al*. (1991)). The GP method produces a predictive distribution of the form error estimate, allowing a decision maker to take into account the uncertainty from the model and sampling.

One more note is on the random error term ε in the model. Dowling *et al*. (1997) mentioned that the rule of thumb in practice is that one may ignore measurement errors if the tolerance size is ten times larger than them. The CMM we used is a Sheffield Discovery II D-8. Its calibrated volumetric accuracy and repeatability are 4.7 and 1.66 μm in range, respectively, suggesting the combined uncertainty is around 6 μm. Compared with the form errors of 0.052 mm for straight and 0.43 mm for round features the above general rule certainly holds for round features and approximately holds for straight features (about 8 times). Thus, our treatment of attributing all the random error to the manufacturing process is reasonable for the products we analyzed. However, some high-precision manufacturing processes, such as grinding, lapping and honing, have a typical tolerance limit of a few microns (for example, ± 8 μm for grinding). Then, the above rule will not be satisfied. Therefore, in general engineers need to consider, and eventually to eliminate, the influence of the measurement error to reduce the false positives in quality control. We believe that the current GP model can be extended to include the measurement error, but it requires repeated measurements to enable differentiating measurement errors from random manufacturing errors.

Acknowledgments

The authors gratefully acknowledge financial support from the NSF under grant CMMI-0348150 and from the State of Texas Advanced Technology Program under grant 000512-0237-2003. The authors also appreciate the editor and the referees for their valuable comments and suggestions.

References

Banerjee, S., Carlin, B. and Gelfand, A. (2004) *Hierarchical Modeling and Analysis for Spatial Data*, Chapman & Hall/CRC, Boca Raton, FL.

Bernardo, M., Buck, R., Liu, L., Nazaret, W., Sacks, J. and Welch, W. (1992) Integrated circuit design optimization using a sequential strategy. *IEEE Transactions on Computer-Aided Design of Integrated Circuits and Systems*, **11**, 361–372.

Chang, S. and Ho, S. (2001) Multivariate statistical process control for inspection data from coordinate measuring machines. *International Journal of Industrial Engineering – Theory, Applications and Practices*, **8**, 347–358.

Chen, C. and Liu, C. (2000) A study on analyzing the problem of the spherical form error. *Precision Engineering*, **24**, 119–126.

Cho, N. and Tu, J. (2001) Roundness modeling of machined parts for tolerance analysis. *Precision Engineering*, **25**, 35–47.

Choi, W. and Kurfess, T. (1999a) Dimensional measurement data analysis, part 1: a zone fitting algorithm. *Journal of Manufacturing Science and Engineering*, *Transactions of the ASME*, **121**, 238–245.

Choi, W. and Kurfess, T. (1999b) Dimensional measurement data analysis, part 2: minimum zone evaluation. *Transactions of the ASME*, *Journal of Manufacturing Science and Engineering*, **121**, 246–250.

Cressie, N. and Lahiri, S. (1996) Asymptotics for REML estimation of spatial covariance parameters. *Journal of Statistical Planning and Inference*, **50**, 327–341.

Deng, G., Wang, G. and Duan, J. (2003) A new algorithm for evaluating form error: the valid characteristic point method with the rapidly contracted constraint zone. *Journal of Materials Processing Technology*, **139**, 247–252.

Desta, M., Feng, H. and OuYang, D. (2003) Characterization of general systematic form errors for circular features. *International Journal of Machine Tools & Manufacture*, **43**, 1069–1078.

Dowling, M., Griffin, P., Tsui, K. and Zhou, C. (1995) A comparison of the orthogonal least square and minimum enclosing zone methods for form error estimation. *Manufacturing Review*, **8**, 120–134.

Dowling, M., Griffin, P., Tsui, K. and Zhou, C. (1997) Statistical issues in geometric feature inspection using coordinate measuring machines. *Technometrics*, **39**, 3–17.

Dowling, M., Griffin, P. and Zhou, C. (1993) Statistical issues in geometric tolerance verification using coordinate measuring machines. Research report J-90-2, School of Industrial and Systems Engineering, Georgia Institute of Technology, Atlanta, GA.

Fan, K. and Lee, J. (1999) Analysis of minimum zone sphericity error using minimum potential energy theory. *Precision Engineering*, **23**, 65–72.

Gaudard, M., Karson, M., Linder, E. and Sinhai, D. (1999) Bayesian spatial prediction. *Environmental and Ecological Statistics*, **6**, 147–171.

Hardle, W. and Simar, L. (2003) *Applied Multivariate Statistical Analysis*, Springer, New York, NY.

Henke, R., Summerhays, K., Baldwin, J., Cassou, R. and Brown, C. (1999) Methods for evaluation of systematic geometric deviations in machined parts and their relationships to process variables. *Precision Engineering*, **23**, 273–292.

Huang, J. (1999a) An exact minimum zone solution for sphericity evaluation. *Compute Aided Design*, **31**, 845–853.

Huang, J. (1999b) An exact solution for the roundness evaluation problems. *Precision Engineering*, **23**, 2–8.

Hulting, F. (1995) Comment: an industrial view of coordinate measurement data analysis. *Statistica Sinica*, **5**, 191–204.

Hulting, F. (1997) Discussion: statistical issues in geometric feature inspection using coordinate measuring machines. *Technometrics*, **39**, 18–20.

Kurfess, T., Banks, D. and Wolfson, J. (1996) A multivariate statistical approach to metrology. *Transactions of the ASME, Journal of Manufacturing Science and Engineering*, **118**, 652–657.

Namboothiri, V. and Shunmugam, M. (1998) Form error evaluation using L_1-approximation. *Computer Methods in Applied Mechanics and Engineering*, **162**, 133–149.

Samuel, G. and Shunmugam, M. (1999) Evaluation of straightness and flatness using computational geometric techniques. *Computer Aided Design*, **31**, 829–843.

Samuel, G. and Shunmugam, M. (2000) Evaluation of circularity from coordinate and form data using computational geometric techniques. *Precision Engineering*, **24**, 251–263.

Santner, T., Williams, B. and Notz, W. (2003) *The Design and Analysis of Computer Experiments*, Springer, New York, NY.

Shunmugam, M. (1987) New approach for evaluating form errors of engineering surfaces. *Computer Aided Design*, **19**, 368–374.

Shunmugam, M. (1991) Criteria for computer-aided form evaluation. *Transactions of the ASME, Journal of Engineering for Industry*, **113**, 233–238.

Stout, K., Davis, E. and Sullivan, P. (1990) *Atlas of Machined Surfaces*, Chapman & Hall, London, UK.

Suen, D. and Chang, C. (1997) Application of neural network interval regression method for minimum zone straightness and flatness. *Precision Engineering*, **20**, 196–207.

Traband, M., Medeiros, D. and Chandra, M. (2004) A statistical approach to tolerance evaluation for circles and cynlinders. *IIE Transactions*, **36**, 777–785.

Weber, T., Motavalli, S., Fallahi, B. and Cheraghi, S. (2002) A unified approach to form error evaluation. *Journal of the International Societies for Precision Engineering and Nanotechnology*, **26**, 269–278.

Weckenmann, A., Heinrichowski, M. and Mordhorst, H. (1991) Design of gauges and multipoint measuring systems using coordinate-measuring-machine data and computer simulation. *Precision Engineering*, **13**, 203–207.

Wolfinger, R., Tobias, R. and Sall, J. (1994) Computing Gaussian likelihoods and their derivatives for general linear mixed models. *SIAM Journal of Scientific Computing*, **15**, 1294–1310.

Woo, T. and Hsieh, C. (1997) Discussion: statistical issues in geometric feature inspection using coordinate measuring machines. *Technometrics*, **39**, 20–22.

Yang, T. and Jackman, J. (2000) Form error estimation using spatial statistics. *Transactions of the ASME, Journal of Manufacturing Science and Engineering*, **122**, 262–272.

Yang, B. and Menq, C. (1993) Compensation for form error of end-milled sculptured surfaces using discrete measurement data. *International Journal of Machine Tools & Manufacture*, **33**, 725–740.

Yeh, K.-M., Ni, J. and Hu, S. (1994) Adaptive sampling and identification of feature deformation for tolerance evaluation using coordinate measuring machines. Technical Report, S. M. Wu, Manufacturing Research Laboratory, Dept. of Mechanical Engineering and Applied Mechanics, University of Michigan, Ann Arbor, MI.

Zhu, X., Ding, H. and Wang, M. (2004) Form error evaluation: an iterative reweighted least squares algorithm. *Transactions of the ASME, Journal of Manufacturing Science and Engineering*, **126**, 535–541.

Zimmerman, D. and Harville, D. (1991) A random field approach to the analysis of field-plot experiments and other spatial experiments. *Biometrics*, **47**, 223–229.

Appendix

We here illustrate how to implement the procedures to determine the ideal geometric form (as in Section 3) for two commonly used geometric features, straight and round features.

A1. *Straight features*

For a straight feature, the nominal geometry $M(\mathbf{0},\ \phi^*)$ is $y = 0$, and the general geometry shape $M(\boldsymbol{\theta}, \phi)$ is $y = \delta + \psi x$ (Fig. 4(a)), where $\boldsymbol{\theta} = (\delta, \psi)$ is the location parameter with δ representing translation and ψ representing rotation. In this case, the dimension parameter ϕ degenerates. So $\boldsymbol{\beta} = \boldsymbol{\theta} = (\delta, \psi)$. For a point $\mathbf{n}_i = (x_i, 0)^{\mathrm{T}}$ on the nominal feature $y = 0$, the approach direction is $\mathbf{v}_i = (0, -1)^{\mathrm{T}}$. After solving for the intersection between $y = \delta + \psi x$ and the vertical line $x = x_i$ and then calculating the vector inner product in step (4), we have $\mathbf{f}(x_i, \boldsymbol{\beta})^{\mathrm{T}}\mathbf{v}_i = (x_i, \delta + \psi x_i) \cdot (0, -1)^{\mathrm{T}} = -\delta - \psi x_i$.

A2. *Round features*

For straight features, y is an explicit function of x. However this is not the case for a round feature. Denote the round feature's nominal radius by r_0 and the actual radius by r. As illustrated in Fig. 4(b), the nominal geometry $M(\mathbf{0},\ \phi^*)$ is $x^2 + y^2 = r_0^2$ and the general geometric shape $M(\boldsymbol{\theta}, \phi)$ is $(x - x_0)^2 + (y - y_0)^2 = r^2$, where the location parameter $\boldsymbol{\theta}$ only consists of the translation of the center, i.e., (x_0, y_0), because a round feature is invariant under rotation. The dimension parameter ϕ is the radius r. Thus, $\boldsymbol{\beta} = (x_0,\ y_0,\ r)$. Given the nominal feature $M(\mathbf{0},\ \phi^*)$, we will have $\mathbf{n}_i = (r_0 \cos\tau_i, r_0 \sin\tau_i)^{\mathrm{T}}$and

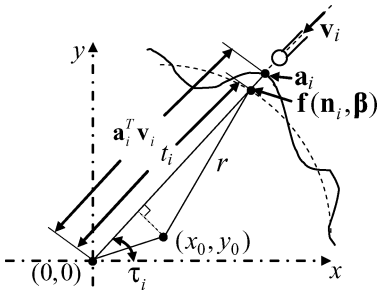

Fig. A1. Triangle relationship for a round feature.

$\mathbf{v}_i = (-\cos\tau_i, -\sin\tau_i)^{\mathrm{T}}$, where τ_i is the polar angle. Consequently, $\mathbf{f}(\mathbf{n}_i, \boldsymbol{\beta})$ is the intersection point of $(x - x_0)^2 + (y - y_0)^2 = r^2$ and the line passing through (0, 0) and $\mathbf{n}_i = (r_0 \cos\tau_i, r_0 \sin\tau_i)^{\mathrm{T}}$, i.e., the solution of the following equations:

$$\begin{cases} (f_{x_i} - x_0)^2 + (f_{y_i} - y_0)^2 = r^2, \\ \frac{f_{y_i}}{f_{x_i}} = \tan\tau_i, \end{cases} \tag{A1}$$

where (f_{x_i}, f_{y_i}) are the two coordinates of the intersection points. Notice that a circle has two intersection points with a line. Pick the first intersection point according to the approaching path of the probe as the final solution (f_{x_i}, f_{y_i}). In this way, we can numerically calculate $\mathbf{f}(\mathbf{n}_i, \boldsymbol{\beta})^{\mathrm{T}}\mathbf{v}_i = -f_{x_i}\cos\tau_i - f_{y_i}\sin\tau_i$ for any given $\mathbf{n}_i$.

For the value of $\mathbf{f}(\mathbf{n}_i, \boldsymbol{\beta})^{\mathrm{T}}\mathbf{v}_i$, we may calculate it via a geometrical method for this roundness feature: As illustrated in Fig. (A1), $\mathbf{f}(\mathbf{n}_i, \boldsymbol{\beta})^{\mathrm{T}}\mathbf{v}_i$ is the t_i in a triangle constructed from the three points: $\mathbf{f}(\mathbf{n}_i, \boldsymbol{\beta})$, (x_0, y_0) and (0, 0) (a similar triangle was utilized in Traband *et al.* (2004)). Solving this triangle, we get $\mathbf{f}(\mathbf{n}_i, \boldsymbol{\beta})^{\mathrm{T}}\mathbf{v}_i = -x_0\cos\tau_i - y_0\sin\tau_i - \sqrt{r^2 - (x_0\sin\tau_i - y_0\cos\tau_i)^2}$.

Biographies

Haifeng (Heidi) Xia received her B.S. degree in International Enterprise Management and her M.S. degree in Management Science and Engineering from Tianjin University, China in 2000 and in 2002, respectively. She is currently a Ph.D. candidate in Industrial and Systems Engineering at Texas A&M University, College Station, TX. Her research focuses on multi-scale/multi-resolution modeling and analysis as well as its applications in dimensional quality control, nanotechnology and remote sensing. She received the 2007 Best Student Paper Award sponsored by the INFORMS Section on Quality, Statistics and Reliability. She is a student member of INFORMS, IIE and ASA.

Yu Ding received a B.S. degree in Precision Engineering from the University of Science and Technology of China in 1993, an M.S. in Precision Instruments from Tsinghua University, China in 1996, an M.S. in Mechanical Engineering from the Pennsylvania State University in 1998, and a Ph.D. in Mechanical Engineering from the University of Michigan in 2001. He is currently an Associate Professor in the Department of Industrial and Systems Engineering at Texas A&M University. His research interests are in the area of quality engineering and applied statistics. His current research is sponsored by the National Science Foundation, the Department of Homeland Security, the State of Texas, and industry. He has received a number of awards for his work, including an *IIE Transactions* Best Paper Award in 2006, the CAREER Award from the National Science Foundation in 2004, and a Best Paper Award from the ASME Manufacturing Engineering Division in 2000. He currently serves as a Department Editor of *IIE Transactions* and an Associate Editor of *IEEE Transactions on Automation Science and Engineering*. He is a member of IIE, INFORMS, IEEE, and ASME.

Jyhwen Wang is an Associate Professor in the Department of Engineering Technology and Industrial Distribution at Texas A&M University. His research interest is in the areas of design and manufacturing with a focus on geometric tolerancing and material processing technologies. He received his B.S. in Industrial Engineering from Tunghai University (Taiwan), M.S. in Industrial Engineering and Operations Research from Syracuse University, M.Eng. in Manufacturing Engineering, and Ph.D. in Mechanical Engineering from Northwestern University. Before joining Texas A&M University, he was a researcher and R&D manager at the Weirton Steel Technology Center.